Phonon impact on optical control schemes of quantum dots: Role of quantum dot geometry and symmetry

S. Lüker, T. Kuhn, and D. E. Reiter
Institut für Festkörpertheorie, Universität Münster, Wilhelm-Klemm-Str. 10, 48149 Münster, Germany
(Received 11 October 2017; published 18 December 2017)

Phonons strongly influence the optical control of semiconductor quantum dots. When modeling the electron-phonon interaction in several theoretical approaches, the quantum dot geometry is approximated by a spherical structure, though typical self-assembled quantum dots are strongly lens-shaped. By explicitly comparing simulations of a spherical and a lens-shaped dot using a well-established correlation expansion approach, we show that, indeed, lens-shaped dots can be exactly mapped to a spherical geometry when studying the phonon influence on the electronic system. We also give a recipe to reproduce spectral densities from more involved dots by rather simple spherical models. On the other hand, breaking the spherical symmetry has a pronounced impact on the spatiotemporal properties of the phonon dynamics. As an example we show that for a lens-shaped quantum dot, the phonon emission is strongly concentrated along the direction of the smallest axis of the dot, which is important for the use of phonons for the communication between different dots.

DOI: 10.1103/PhysRevB.96.245306

I. INTRODUCTION

In the optical control of semiconductor quantum dots (QDs) the coupling to phonons plays a vital role [1,2]. Nowadays, the optical control of excitons and biexcitons in single QDs can be performed experimentally by various techniques and the results clearly demonstrate the influence of phonons. Examples are the phonon-induced damping of Rabi rotations in the case of resonant driving of the QD [3], chirp-dependent phonon damping of the adiabatic rapid passage induced by chirped laser pulses [4–6], phonon-assisted state preparation by detuned excitation [7–11], and the polarization decay in four-wave mixing signals [12,13]. Also, for QDs coupled to a quantized cavity light field, phonons play an important role [14–18]. To theoretically simulate the phonon influence different theoretical approaches have been developed, identifying the coupling to longitudinal acoustic (LA) phonons as typically being the dominant mechanism. Without optical excitation, the system can be described by the independent Boson model, which is exactly solvable. In the phonon-free case, the optically driven QD can also be exactly solved using the semiconductor Bloch equations. When both light field and phonons are active, an exact solution cannot be found anymore and approximations or numerical methods have been developed. Examples are different types of master-equation approaches [19–22], time-convolutionless methods [23,24], correlation expansion techniques [25–28], and path integral formulations [29–31]. The methods rely on different levels of approximations coming with different advantages and disadvantages. In particular, the computational costs of the different methods can greatly vary. In order to reduce the computational costs, in many cases, the approximation of a spherical QD has been made. However, fabrication techniques like, e.g., the Stranski-Krastanov growth mode for self-assembled QDs typically lead to rather lens-shaped geometries, as has also been confirmed by many experimental measurements [32,33]. Nevertheless, various recent combined experimental-theoretical studies on single QDs, in which the theoretical calculations have been based on a spherical dot approximation, have shown an excellent agreement between theory and experiment [3,5–7]. In this paper, we analyze the impact of the approximation of spherical symmetry for simulations of the phonon influence on the dynamics of optically excited QDs.

For a spherical QD, the electron-phonon coupling matrix element only depends on the modulus of the phonon wave vector, which allows one to exploit symmetry arguments to reduce the number of independent variables and thereby the computational cost. In contrast, for a lens-shaped QD, at least two directions have to be taken into account, which often increases the number of variables and the computational cost considerably. In this paper, we provide a direct comparison between a lens-shaped and a spherical QD using the same approximations in the theoretical model. To be specific, we here explicitly compare calculations performed for a spherical and a lens-shaped QD within a correlation expansion [26,27,31] and show that the optically induced electronic properties of the lens-shaped system are perfectly reproduced by a model involving spherical symmetry. As an example we compare the occupation under resonant and chirped excitation. We furthermore show that for each spectral density we can find a spherically symmetric effective confinement potential, which reproduces the spectral density resulting in the same effects on the electronic properties. In addition, we show that the same spectral density can be well approximated by rather simple spherical models with only very few parameters.

On the other hand, when considering the phonon system, the symmetry properties of the QD have a great impact. Using the correlation expansion, we calculate the dynamics of the phonons created during and immediately after the optical excitation [34,35]. The rapid generation of the exciton leads to the formation of a wave packet leaving the QD region [12,36]. For a spherical QD, the generated wave packet retains the spherical symmetry of the QD. For a lens-shaped QD, the wave packet generation reflects the QD symmetry [37], the strongest wave packet emission being in the direction of the smallest size.

II. THEORETICAL BACKGROUND

To study the influence of phonons on the QD exciton system, we make use of the standard two-level model of a strongly confined QD consisting of the ground state $|g\rangle$ at energy 0 and the exciton state $|x\rangle$ at energy $\hbar\omega$ [1,27]. The Hamiltonian for the electronic part of the system can be written as

$$H_{el} = \hbar\omega|x\rangle\langle x| - \mathbf{E}\cdot\mathbf{P}. \tag{1}$$

The second term describes the coupling of the polarization

$$\mathbf{P} = \mathbf{M}|g\rangle\langle x| + \mathbf{M}^*|x\rangle\langle g|, \tag{2}$$

$\mathbf{M}$ being the dipole matrix element, to the light field $\mathbf{E}$, which is treated in dipole and rotating wave approximation.

The phonon part of the system consists of the free phonon part and the electron-phonon interaction described by

$$H_{ph} = \hbar\sum_{\mathbf{q}}\omega_{\mathbf{q}}b_{\mathbf{q}}^\dagger b_{\mathbf{q}} + \hbar|x\rangle\langle x|\sum_{\mathbf{q}}(g_{\mathbf{q}}b_{\mathbf{q}} + g_{\mathbf{q}}^* b_{\mathbf{q}}^\dagger), \tag{3}$$

with $b_{\mathbf{q}}$ ($b_{\mathbf{q}}^\dagger$) being the annihilation (creation) operator for a phonon with wave vector $\mathbf{q}$. We consider LA phonons with linear dispersion $\omega_{\mathbf{q}} = c_{\mathrm{LA}}q$ (c_{LA} being the sound velocity). $g_{\mathbf{q}} = g_{\mathbf{q}}^e - g_{\mathbf{q}}^h$ is the coupling matrix element for deformation potential coupling given by

$$g_{\mathbf{q}}^{e/h} = \sqrt{\frac{q}{2V\rho\hbar c_{\mathrm{LA}}}}D_{e/h}F_{\mathbf{q}}^{e/h} \tag{4}$$

for electrons (e) and holes (h). The constants are the normalization volume V, the mass density ρ, and the deformation potential coupling constant $D_{e/h}$ for electrons/holes. The spatial confinement of the carriers enters via the form factors

$$F_{\mathbf{q}}^{e/h} = \int d^3r\,|\psi^{e/h}(\mathbf{r})|^2\,e^{i\mathbf{q}\cdot\mathbf{r}} \tag{5}$$

depending on the envelope function $\psi^{e/h}(\mathbf{r})$ of electrons/holes. For the QD, we assume a harmonic confinement potential. Considering a lens-shaped QD with the localizations length $a_z^{e/h}$ in the z-direction and $a_r^{e/h}$ in the (x,y)-plane (with $a_z^{e/h} < a_r^{e/h}$), the form factor reads

$$F_{\mathbf{q}}^{e/h} = \exp\left\{-\tfrac{1}{4}\left(q_z^2\left(a_z^{e/h}\right)^2 + q_r^2\left(a_r^{e/h}\right)^2\right)\right\}, \tag{6}$$

where q_z is the wave vector component in z direction, q_r is the modulus of the in-plane wave vector, and $q = \sqrt{q_r^2 + q_z^2}$. In the case of a spherical QD, we have $a_z^{e/h} = a_r^{e/h} = a^{e/h}$ simplifying the form factor to

$$F_{\mathbf{q}}^{e/h} = \exp\left[-\tfrac{1}{4}q^2(a^{e/h})^2\right]. \tag{7}$$

Here, we already see that the numerical implementation of a spherical QD relies only on the modulus of the wave vector q, while for a lens-shaped QD, a discretization of both q_z and q_r is required. If not denoted otherwise, we use standard GaAs parameters (see Table I), which, assuming the same confinement potential for electrons and holes, give the ratio of the localization length between electron and hole to $a^h/a^e = (m_e/m_h)^{1/4} = 0.87$ [38].

Using the Hamiltonian given above the equations of motion are set up. In the density matrix formalism, starting from the basic electronic and phononic variables, exciton occupation $f = \langle|x\rangle\langle x|\rangle$, excitonic polarization $p = \langle|g\rangle\langle x|\rangle$, coherent phonon amplitudes $B_{\mathbf{q}} = \langle b_{\mathbf{q}}\rangle$, and phonon occupations $n_{\mathbf{q},\mathbf{q}'} = \langle b_{\mathbf{q}}^\dagger b_{\mathbf{q}'}\rangle$, the many-body nature of the carrier-phonon coupling leads to an infinite hierarchy of equations of motion. In the higher orders, phonon-assisted quantities appear like $\langle b_{\mathbf{q}}^\dagger|x\rangle\langle x|\rangle$ or $\langle b_{\mathbf{q}}^\dagger b_{\mathbf{q}}^\dagger|x\rangle\langle x|\rangle$. In the correlation expansion, the correlations of the phonon-assisted quantities are neglected at a certain order. Obviously, the dimension of $\mathbf{q}$ is directly related to the dimension of the phonon-assisted quantities. Hence the restriction to a one-dimensional $\mathbf{q}$ goes along with an immense saving of computational cost. In the following, we will employ a fourth-order correlation expansion, which has proven to simulate experimental results very well [1,5,6].

TABLE I. Material parameters.

Longitudinal sound velocity	c_{LA}	5.1 nm ps^{-1}
Mass density	ρ	5.31 g cm^{-3}
Electron deformation potential	D_e	7 eV
Hole deformation potential	D_h	−3.5 eV
Effective electron mass	m_e	$0.067m_0$
Effective hole mass	m_h	$0.110m_0$
Free electron mass	m_0	9.1×10^{-31} kg

III. SPECTRAL DENSITY

The phonon spectral density provides a measure for the coupling efficiency between the phonons and the carriers. It is defined as

$$J(\omega) = \sum_{\mathbf{q}}|g_{\mathbf{q}}|^2\delta(\omega-\omega_{\mathbf{q}}). \tag{8}$$

For a spherical QD with $a^e = a^h = a$, an analytical expression for the spectral density is available [39,40], which has the form

$$J(\omega) = A\omega^3\exp\left(-\omega^2/\omega_c^2\right), \tag{9}$$

where ω_c is the cutoff frequency determined by the size of the QD and A is a measure for the coupling strength. For the coupling given in Eq. (4) these parameters are given by

$$A = \frac{(D_e - D_h)^2}{4\pi^2\rho\hbar c_{\mathrm{LA}}^5}, \quad \omega_c = \sqrt{2}\frac{c_{\mathrm{LA}}}{a}.$$

The spectral densities of differently shaped QDs are compared in Fig. 1. In Fig. 1(a), we keep the in-plane localization length of the electrons fixed to $a_r^e = 5.0$ nm and vary the size in z-direction a_z^e. The corresponding localization lengths of the holes are taken to be $a^h = 0.87a^e$. All curves exhibit a nonmonotonic behavior with a pronounced maximum. Phonons with energies $E = \hbar\omega_{\mathbf{q}}$ in the region around the maximum bear the major impact on the carrier dynamics. For $a_z^e = 5$ nm, the QD is spherical and the maximum is at about 1.2 meV. The dashed curve shows the analytical equation (9), the fit parameters are $A = 0.036$ ps^2 and $\omega_c = 1.52$ ps^{-1}. Though the considered dot does not fulfill $a^e = a^h$, the analytical formula leads to an excellent agreement with the phonon spectral density of the spherical QD. The cutoff frequency of the fit corresponds to a localization length of

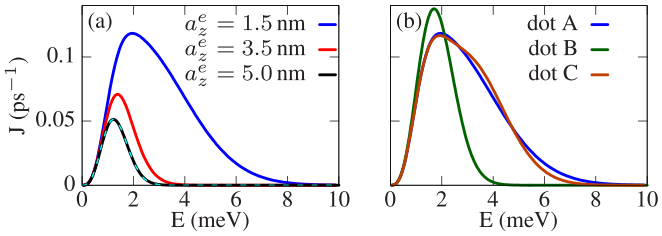

FIG. 1. Phonon spectral density for (a) a QD with an in-plane size $a_r^e = 5.0$ nm and different heights $a_z^e = 1.5$, 3.5, and 5.0 nm. The dashed line is the spectral density according to Eq. (9). (b) Phonon spectral density for QDs A, B, and C as explained in the text.

4.75 nm, which is between the values for electrons (5 nm) and holes (4.35 nm). With decreasing height, the QD becomes more lens-shaped. In the spectral density, the maximum shifts to higher energies with 1.4 meV for $a_z^e = 3.5$ nm and 2.0 meV for $a_z^e = 1.5$ nm. Also, the high-energy part of the spectral density changes and becomes extended to larger energies. This widening reflects the fact that the wave functions are now narrower in the z direction. Note that on the low-energy side the spectral density is the same for all three curves, because here the behavior is dominated by the cubic dependence resulting from the coupling matrix element and the phonon density of states, reflecting the superohmic nature of the carrier-phonon coupling.

We are now looking for a spherical QD, which gives the same spectral density as for an arbitrary lens-shaped dot. Because the phonon spectral density is a one-dimensional quantity depending only on the frequency ω, it is possible to reproduce an arbitrary phonon spectral density by a spherically shaped QD even with equal localization lengths of electrons and holes. To show this, we assume equal and isotropic form factors $F_q^e = F_q^h = F_q$. Then the spectral density reads

$$J(\omega) = \sum_{\mathbf{q}} \frac{q}{2V\rho\hbar c_{\mathrm{LA}}}(D_e - D_h)^2 F_q^2 \delta(\omega - \omega_{\mathbf{q}}) = \frac{\omega^3}{4\pi^2\rho\hbar c_{\mathrm{LA}}^5}(D_e - D_h)^2 F^2_{\frac{\omega}{c_{\mathrm{LA}}}}. \tag{10}$$

Taking the spectral density $J(\omega)$ of an arbitrary QD as given, we thus obtain a spherically symmetric form factor

$$F_q = \left[\frac{4\pi^2\rho\hbar c_{\mathrm{LA}}^2}{q^3(D_e - D_h)^2} J(c_{\mathrm{LA}} q)\right]^{1/2},$$

which reproduces exactly the given spectral density. Using Eq. (5), we obtain the square modulus of the corresponding wave function by inverse Fourier transformation via

$$|\psi(r)|^2 = \frac{1}{(2\pi)^3}\int d^3q\, F_q\, e^{-i\mathbf{q}\cdot\mathbf{r}} = \int_0^\infty \frac{q\sin(qr)}{2\pi^2 r} F_q\, dq.$$

Note that we here took into account already the spherical symmetry. Considering the ground state, the wave function does not have nodes and we can assume $\psi(r) = \sqrt{|\psi(r)|^2} = r^{-1}u(r)$. The function $u(r)$ satisfies a radial Schrödinger equation

$$\left(-\frac{\hbar^2}{2m_e}\frac{d^2}{dr^2} + V(r)\right)u(r) = E\,u(r) \tag{11}$$

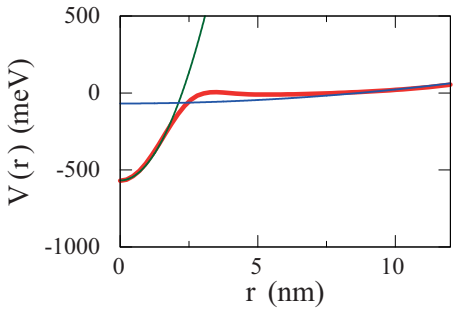

FIG. 2. Spherically symmetric effective potential (red line) obtained from Eq. (12) for a lens-shaped QD with $a_r^e = 5$ nm and $a_z^e = 1.5$ nm. For comparison the parabolic electron potentials are shown for the in-plane (blue line) and out-of-plane (green line) directions.

with an effective potential $V(r)$. Setting the energy E to zero, the potential follows from

$$V(r) = \frac{\hbar^2}{2m_e}\frac{1}{u}\frac{d^2u}{dr^2}. \tag{12}$$

Equation (12) allows us to calculate for a given phonon spectral density of a nonspherical QD a fictitious spherically symmetric effective potential. By construction, the wave function of this fictitious QD exactly reproduces the phonon spectral density of the original nonspherical QD. It should be noted that the choice of the electron mass m_e in Eqs. (11) and (12) is arbitrary; one might also choose the hole mass or any other mass, which would simply scale the potential.

Already for lens-shaped dots with harmonic confinement, an analytical solution of Eq. (12) is lengthy and not very instructive. Figure 2 shows the numerically calculated effective potential $V(r)$ reproducing the phonon spectral density of the lens-shaped QD with $a_r^e = 5$ nm, $a_z^e = 1.5$ nm, and $a^h/a^e = 0.87$ of Fig. 1(a) (blue curve). The thick red line is the effective potential calculated by the procedure outlined above. Obviously, the exciton potential is not anymore harmonic, but is essentially composed of two parts that exhibit a harmonic shape. For comparison, the in-plane (blue) and out-of-plane (green) potentials of the lens-shaped QD are marked by thin lines. (Note that the potentials for electrons and holes are the same.) For $r \to 0$, the effective potential is dominated by the potential in z-direction showing a steep harmonic behavior. For larger distances, the in-plane harmonic potential dominates the effective potential. In between, the potential is continuous with a local maximum around the region where the harmonic potentials cross.

While the procedure described above allows us to construct a spherically symmetric QD, which exactly reproduces the phonon spectral density of an arbitrarily shaped QD, we will now show that for lens-shaped QDs with harmonic confinement potentials the spectral density can even be well approximated by spherically symmetric Gaussian wave functions for electrons and holes. In the following, we will use the most strongly lens-shaped QD in Fig. 1(a) (blue curve) as a reference and call this QD A. In Fig. 1(b), we compare this QD with two spherically symmetric ones, QD B and QD C. The parameters of these three dots are

QD A: $a_r^e = 5.0$ nm, $a_z^e = 1.5$ nm, $a^h/a^e = 0.87$;
QD B: $a_r^e = a_z^e = 3.6$ nm, $a^h/a^e = 0.87$;
QD C: $a_r^e = a_z^e = 4.7$ nm, $a^h/a^e = 0.40$.

QD B is a spherical dot with the standard localization length ratio $a^h/a^e = 0.87$ and a radial localization length $a^e = 3.6$ nm chosen in such a way that it has the same Huang-Rhys factor [41–43] as QD A, i.e., the same value for

$$S = \int \frac{J(\omega)}{\omega^2} d\omega. \tag{13}$$

The Huang-Rhys factor determines the polaron shift and is a measure for the total coupling strength.

Figure 1(b) shows that the agreement is not very satisfying. While for energies up to the maximum the spectral density is well reproduced, this spherical QD completely fails in reproducing the high-energy tail of the spectral density.

However, when we allow the confinement ratio a^h/a^e to vary, we find a rather good agreement, as shown for QD C using $a^e = 4.7$ nm and $a^h/a^e = 0.40$. This QD, modeled by just two isotropic Gaussian wave functions, is able to reproduce both the rise of the spectral density to the maximum at 2.0 meV and the long tail up to around 8 meV. Only small differences in the high-energy tail of the spectral density between QD A and QD C are visible.

IV. PHONON INFLUENCE ON THE ELECTRONIC SYSTEM

In the next step, we compare the influence of the QD shape on the optically excited exciton occupation of a QD using the lens-shaped QD A and the spherical QDs B and C. Note that a spherical QD confined by the effective potential calculated via Eq. (12) exactly reproduces the results of the lens-shaped QD A (not shown).

The standard example for optical excitations are Rabi rotations, which recently have been measured for a pulse area up to 12π [3,44]. Here we consider the excitation with a Gaussian laser pulse described by the instantaneous Rabi frequency (pulse envelope)

$$\Omega(t) = \frac{\Theta}{\sqrt{2\pi}\tau} \exp\left(-\frac{t^2}{2\tau^2}\right) \tag{14}$$

with pulse area Θ, pulse length $\tau = 4$ ps, and frequency ω being resonant with the exciton transition. In Fig. 3(a), the Rabi rotations for the three QDs A, B, and C are shown. For pulse areas up to about 12π, we observe a damping of the Rabi rotations with increasing pulse area, which is essentially the same for all three QDs. Subsequently, the amplitude of the rotations increases again, which is more pronounced for QD B, while QDs A and C remain to be in almost perfect agreement. This growth of the amplitude indicates the regime of the reappearance of Rabi rotations, which has been theoretically predicted [31,45], however, not yet clearly seen experimentally, mainly because of the very high pulse areas necessary to enter this regime.

More insight in the pulse area dependence of Rabi rotations for the different QDs can be obtained in the dressed state picture. The dressed states are the eigenstates of the coupled QD-light system [1,35]. In the dressed state picture, phonons give rise to transitions between the dressed states [6,35,46] if

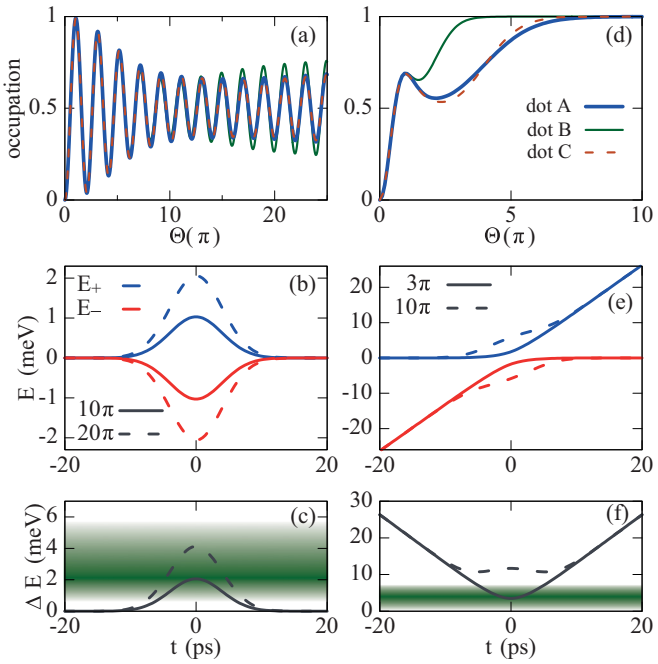

FIG. 3. (a) Final occupation of the exciton state as a function of the pulse area for resonant excitation with a 4-ps Gaussian laser pulse for dot A (blue line), dot B (green line), and dot C (red dashed line). (b) Instantaneous eigenenergies E_+ and E_- for excitation with a resonant Gaussian 10π pulse (solid lines) and 20π pulse (dashed lines). (c) Energy splitting $\Delta E = E_+ - E_-$ of the eigenenergies for the 10π pulse (solid line) and 20π pulse (dashed line); the green-shaded area highlights the strength of the phonon spectral density as a function of the energy ΔE. (d)–(f) Same as left panel, but for excitation with a negatively chirped laser pulse with $\alpha = -0.5$ ps^2 and $\tau_0 = 80$ fs. In (d) and (f), the curves refer to pulse areas of 3π (solid lines) and 10π (dashed lines).

the actual splitting is comparable to the energy range covered by the phonon spectral density. The dressed states as function of time for the Gaussian excitation with a pulse area of 10π and 20π are presented in Fig. 3(b), while Fig. 3(c) shows the energy splitting $\Delta E = E_+ - E_-$. The green-shaded area highlights the strength of the phonon spectral density of QD A as a function of the energy ΔE with its maximum at about 2 meV. For the Gaussian pulse, the splitting also takes a Gaussian curve with a maximum at the time of the pulse maximum. Before and after the laser pulse the eigenenergies are degenerate. Hence phonons from a large energy spectrum starting from 0 up to the maximal splitting contribute to the damping. For a pulse area of 10π, the splitting reaches the maximum value of the spectral density [see Fig. 3(c)]. Therefore, up to such pulse areas, the damping of the Rabi rotations increases. Up to the maximum, the phonon spectral densities of the three dots are very similar leading also to a very similar behavior of the Rabi rotations. For a pulse area of 20π, the splitting reaches values where the spectral density is already considerably reduced compared to its maximal value leading to the observed increased amplitude of the Rabi rotations. In this energy range, the spectral density of QD B is much smaller than for QDs A and C explaining why QD B exhibits larger Rabi rotations than the other dots. However, from Fig. 3(c), we also note that even if the energy splitting at the pulse maximum is already far beyond the

maximum of the spectral density, due to the degeneracy before and after the laser pulse, there is always a time where the energy splitting of the dressed states passes by the maximum of the phonon spectral density, which yields the main contribution to the phonon-induced damping of the Rabi rotations.

The second example is an excitation using a chirped laser pulse [47,48], which turned out to be very sensitive to the phonon influence and for which excellent agreement between theory and experiment has recently been shown [5,6]. It is well established that at low temperatures only negatively chirped pulses exhibit a damping due to phonons [4–6,27], hence we concentrate on this case here. The theory for the description of the chirped pulses can be found, e.g., in Refs. [6,27]. Following Ref. [6], we take a resonant Gaussian pulse [Eq. (14)] with initial pulse length of $\tau_0 = 80$ fs and apply a chirp filter with coefficient $\alpha = -0.5\,\mathrm{ps}^2$. As a result, the central frequency of the laser pulse changes linearly with time, while the pulse length is stretched to $\tau = 6.1$ ps, the pulse envelope being given by

$$\Omega(t) = \frac{\Theta}{\sqrt{2\pi\,\tau\,\tau_0}} \exp\left(-\frac{t^2}{2\tau^2}\right). \tag{15}$$

The resulting exciton occupations are shown in Fig. 3(d) for QDs A, B, and C.

For QD A, we find that the occupation rises to a maximum at a pulse area around 1π. Then, the damping sets in resulting in a minimum of the occupation around 2.5π. After the minimum, the occupation rises again and reaches values up to one, i.e., almost perfect exciton generation, showing clearly the reappearance of the ARP effect [6]. The spherical QD C reproduces this behavior well, but some slight deviations from the lens-shaped QD A are seen, which can be attributed to the small differences in the spectral density. Around the minimum, the occupation of dot C is slightly below the occupation of dot A, which is a result of the mismatch of the phonon spectral densities around 4 meV, which promotes a slightly stronger phonon coupling of dot C. On the other hand, the phonon spectral density of dot A exceeds the one of dot B for energies above 6 meV, which leads to a slightly stronger coupling of high energy phonons that slightly reduces the recovery of the occupation to 1 of dot A for $\Theta > 5\pi$.

Dot B is not able to reproduce the found behavior at all, instead the minimum is at a much lower pulse area and also the reappearance occurs at much lower pulse areas. The behavior can again be understood by looking at the dressed states. Due to the transformation to the frame rotating with the instantaneous frequency of the pulse, the energy of one of the eigenstate changes linearly with time while the other remains fixed. The light pulse now leads to an avoided crossing of the two states resulting in a finite splitting between the dressed states at any time [Fig. 3(d)]. Indeed, due to this fact, the low-energy phonons below the minimal splitting (determined by the amplitude of the light at the pulse maximum) cannot contribute to the damping of the ARP at all and the phonon impact is restricted to the high-energy tail of the phonon spectral density. Comparing this to Fig. 1(b), where we indeed found the largest difference for higher energy phonons, it is clear why the ARP is much more sensitive to the QD shape than the Rabi rotations. In Fig. 3(f), the energy splitting for pulse areas of 3π and 10π is plotted together with the energy dependence of the phonon spectral density (green shaded area). We clearly see that for the 10π pulse the energy region of a nonvanishing phonon spectral density is never reached, explaining why here we obtain an essentially perfect exciton generation via the ARP process. The main reason for the different behavior of resonant and chirped excitation in the reappearance regime is thus the fact that for resonant excitation the splitting starts from zero and always passes through the region of strong phonon coupling while for chirped excitation the splitting starts from very large values and, for sufficiently strong pulses, never reaches the region where phonon coupling is efficient.

Altogether, the dot shape has an impact on the carrier-phonon coupling. However, the decisive quantity that describes the phonon coupling is the phonon spectral density. Mathematically speaking, the phonon spectral density is a one-dimensional function depending only on the frequency, where information about the full three-dimensional phonon coupling is lost. Hence it is always possible to find a spherical dot that has the same or a similar phonon spectral density compared to a more realistic lens-shaped QD. Often this is even possible by using rather simple wave functions obtained, e.g., by using the localization length ratio a^h/a^e as a fit parameter. This can be very beneficial by considerably reducing computational costs. This is also of importance when considering systems with more than two states involving, e.g., biexcitons.

We remark that our considerations also hold for other electron-phonon coupling mechanisms like the Fröhlich coupling to optical phonons and the piezoelectric coupling to acoustic phonons. Also, in these cases, the spectral density can be reproduced by a spherically symmetric model. While in the case of Fröhlich coupling the bulk coupling matrix element is again isotropic, such that the formalism can be directly transferred, in the piezoelectric case already the bulk coupling matrix element is anisotropic. Here, introducing an isotropic model requires in addition a suitable angular averaging of the bulk coupling matrix element.

V. PHONON DYNAMICS

We now turn to the dynamics of the phononic system. Though a lens-shaped QD can be substituted by an adapted spherical dot to calculate the carrier dynamics, the phonons generated during the optical control are largely affected by the geometry of the QD. The phonon properties nowadays receive much attention [36], also because new schemes make use of phonons to control QDs. For example, the optical output of a QD can be controlled by surface acoustic waves [49,50] or the lasing properties of QDs can be modulated by strain waves [51]. As an example of the influence of the QD shape on the phonon dynamics, we discuss the properties of the phonon wave packets emitted during the optical excitation of a QD [34,35,37]. For that purpose, we consider the relative volume change, i.e., the divergence of the mean displacement field $\langle \mathbf{u}(\mathbf{r})\rangle$,

$$\frac{\delta V}{V}(\mathbf{r}) = \mathrm{div}\langle \mathbf{u}(\mathbf{r})\rangle = \sum_{\mathbf{q}} \sqrt{\frac{\hbar}{2\rho V \omega_{\mathbf{q}}}} (\langle b_{\mathbf{q}}\rangle e^{i\mathbf{q}\cdot\mathbf{r}} + \langle b_{\mathbf{q}}^{\dagger}\rangle e^{-i\mathbf{q}\cdot\mathbf{r}}), \tag{16}$$

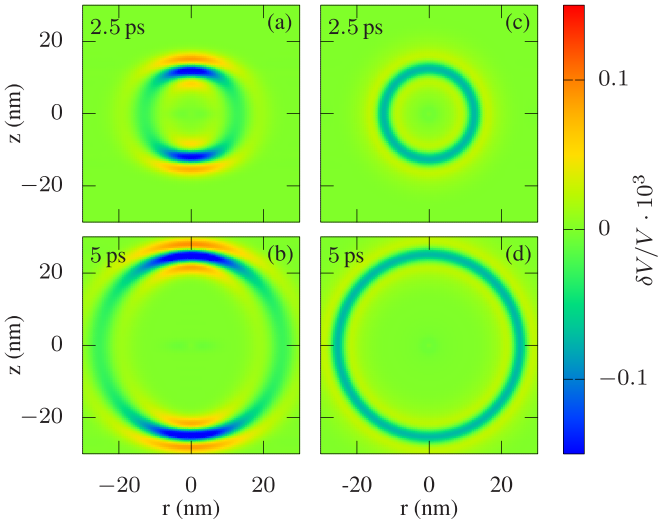

FIG. 4. Relative volume change $\delta V/V$ after an excitation with a 2π pulse for (a), (b) for the lens-shaped QD A and (c), (d) for the spherical dot QD C. (a) and (c) show the wave packet at $t = 2.5$ ps and (b) and (d) at an advanced time $t = 5$ ps.

which describes the change of the lattice unit cells due to the coherent phonon modes. Figure 4 shows the relative volume change of the lattice after the optical excitation of the QD by a Gaussian pulse for the lens-shaped QD A (left) and the spherical QD C (right). The pulse length is chosen to 0.5 ps, which enables an efficient coupling to the phonons [35]. For the pulse area, we take a 2π pulse, resulting in the creation and immediate annihilation of the exciton. Whenever an exciton is present in the dot, the surrounding lattice atoms react on the changed charge configuration by the formation of a polaron, i.e., a static lattice deformation. Because we consider long times after the excitation and de-excitation of the exciton, the polaron has already vanished. However, the rapid creation and destruction of the polaron leads to the emission of a phonon wave packet. The details of the phonon emission can be understood by considering the formation of the polaron [35].

When the polaron is created, a contraction of the lattice unit cells in the QD region occurs, i.e., a negative relative volume variation. The strain that comes along with this contraction is transferred to surrounding lattice cells, which are in turn stretched. Hence the leading edge of the emitted phonon wave packet features a positive volume variation. Afterwards, a front of a negative volume variation follows indicating a lattice contraction similar the polaron. Finally, the trailing edge of the phonon wave packet exhibits again a positive volume variation that is a fingerprint of the destruction of the polaron, i.e., the lattice atoms in the QD area return back to their initial positions, so that the lattice unit cells are stretched again.

Both the spherical and the lens-shaped QD exhibit the same sequence of positive and negative volume variation. However, the emitted wave packet reproduces the symmetry of the QD. In the case of a lens-shaped QD, the symmetry is broken, so that the preferred direction points towards the smallest extension of the dot. Accordingly, in Figs. 4(a) and 4(b), we observe the emission of a phonon wave packet, but it is clearly visible that the amplitude is much stronger in z direction than in the in-plane direction. This can be related to the coupling strength for the phonons, which becomes stronger the smaller the confinement is. For the spherical QD in Figs. 4(c) and 4(d), we see a ring moving outwards, reflecting the spherical shape of the QD. We note that for the case of piezoelectric coupling the anisotropic bulk coupling matrix element introduces an additional anisotropy in the phonon emission besides the anisotropy introduced by the QD geometry [37]. For the Fröhlich coupling to optical phonons, on the other hand, an anisotropic polaron will build up for an antisymmetric QD, however, due to the vanishing group velocity, no phonon wave packet will be emitted into the surrounding material.

The usage of stronger pulses or sequences of pulses can result in the creation of wave packet trains [35] or even squeezed phonons [34], which would be emitted into a direction that is determined by the QD geometry. This shows that by tailoring the QD geometry one gains control over the phonon generation.

VI. CONCLUSION

By explicitly comparing the electron-phonon coupling of a spherical QD and a lens-shaped QD using the same theoretical approach, we draw two conclusions. For the electronic system, it is sufficient to use the spherical symmetry even if the QD shape is more involved. This can be traced back to the fact that the decisive quantity in this case is the phonon spectral density, which is a one-dimensional function, and hence can be exactly reproduced by a radial QD symmetry that is adapted to the properties of the lens-shaped dot. For the phonon system, the actual shape plays an important role in determining the properties of the created phonons. A directed emission of phonons can only be modeled by including the actual shape of the QD. The strongest emission is along the smallest axis of the QD. By performing a direct comparison, we shed new light on the question regarding the influence of the QD geometry on the optical state preparation of self-assembled QDs.

ACKNOWLEDGMENTS

We thank Daniel Wigger and Martin Axt for fruitful discussions.

[1] D. E. Reiter, T. Kuhn, M. Glässl, and V. M. Axt, The role of phonons for exciton and biexciton generation in an optically driven quantum dot, J. Phys. Condens. Matter **26**, 423203 (2014).

[2] A. J. Ramsay, A review of the coherent optical control of the exciton and spin states of semiconductor quantum dots, Semicond. Sci. Technol. **25**, 103001 (2010).

[3] A. J. Ramsay, A. V. Gopal, E. M. Gauger, A. Nazir, B. W. Lovett, A. M. Fox, and M. S. Skolnick, Damping of Exciton Rabi Rotations by Acoustic Phonons in Optically Excited InGaAs/GaAs Quantum Dots, Phys. Rev. Lett. **104**, 017402 (2010).

[4] R. Mathew, E. Dilcher, A. Gamouras, A. Ramachandran, H. Y. S. Yang, S. Freisem, D. Deppe, and K. C. Hall,

Subpicosecond adiabatic rapid passage on a single semiconductor quantum dot: Phonon-mediated dephasing in the strong-driving regime, Phys. Rev. B **90**, 035316 (2014).

[5] T. Kaldewey, S. Lüker, A. V. Kuhlmann, S. R. Valentin, A. Ludwig, A. D. Wieck, D. E. Reiter, T. Kuhn, and R. J. Warburton, Coherent and robust high-fidelity generation of a biexciton in a quantum dot by rapid adiabatic passage, Phys. Rev. B **95**, 161302 (2017).

[6] T. Kaldewey, S. Lüker, A. V. Kuhlmann, S. R. Valentin, J. M.Chauveau, A. Ludwig, A. D. Wieck, D. E. Reiter, T. Kuhn, and R. J. Warburton, Demonstrating the decoupling regime of the electron-phonon interaction in a quantum dot using chirped optical excitation, Phys. Rev. B **95**, 241306 (2017).

[7] J. H. Quilter, A. J. Brash, F. Liu, M. Glässl, A. M. Barth, V. M. Axt, A. J. Ramsay, M. S. Skolnick, and A. M. Fox, Phonon-Assisted Population Inversion of a Single InGaAs/GaAs Quantum Dot by Pulsed Laser Excitation, Phys. Rev. Lett. **114**, 137401 (2015).

[8] F. Liu, L. M. P. Martins, A. J. Brash, A. M. Barth, J. H. Quilter, V. M. Axt, M. S. Skolnick, and A. M. Fox, Ultrafast depopulation of a quantum dot by LA-phonon-assisted stimulated emission, Phys. Rev. B **93**, 161407 (2016).

[9] S. Bounouar, M. Müller, A. M. Barth, M. Glässl, V. M. Axt, and P. Michler, Phonon-assisted robust and deterministic two-photon biexciton preparation in a quantum dot, Phys. Rev. B **91**, 161302 (2015).

[10] P.-L. Ardelt, M. Koller, T. Simmet, L. Hanschke, A. Bechtold, A. Regler, J. Wierzbowski, H. Riedl, J. J. Finley, and K. Müller, Optical control of nonlinearly dressed states in an individual quantum dot, Phys. Rev. B **93**, 165305 (2016).

[11] M. Reindl, K. D. Jöns, D. Huber, C. Schimpf, Y. Huo, V. Zwiller, A. Rastelli, and R. Trotta, Phonon-assisted two-photon interference from remote quantum emitters, Nano Lett. **17**, 4090 (2017).

[12] T. Jakubczyk, V. Delmonte, S. Fischbach, D. Wigger, D. E. Reiter, Q. Mermillod, P. Schnauber, A. Kaganskiy, J.-H. Schulze, A. Strittmatter, S. Rodt, W. Langbein, T. Kuhn, S. Reitzenstein, and J. Kasprzak, Impact of phonons on dephasing of individual excitons in deterministic quantum dot microlenses, ACS Photonics **3**, 2461 (2016).

[13] D. Wigger, Q. Mermillod, T. Jakubczyk, F. Fras, S. Le-Denmat, D. E Reiter, S. Höfling, M. Kamp, G. Nogues, C. Schneider, T. Kuhn, and J. Kasprzak, Exploring coherence of individual excitons in InAs quantum dots embedded in natural photonic defects: Influence of the excitation intensity, Phys. Rev. B **96**, 165311 (2017).

[14] S. Hughes, P. Yao, F. Milde, A. Knorr, D. Dalacu, K. Mnaymneh, V. Sazonova, P. J. Poole, G. C. Aers, J. Lapointe, R. Cheriton, and R. L. Williams, Influence of electron-acoustic phonon scattering on off-resonant cavity feeding within a strongly coupled quantum-dot cavity system, Phys. Rev. B **83**, 165313 (2011).

[15] A. Ulhaq, S. Weiler, C. Roy, S. M. Ulrich, M. Jetter, S. Hughes, and P. Michler, Detuning-dependent mollow triplet of a coherently-driven single quantum dot, Opt. Express **21**, 4382 (2013).

[16] P. Kaer, P. Lodahl, A.-P. Jauho, and J. Mork, Microscopic theory of indistinguishable single-photon emission from a quantum dot coupled to a cavity: The role of non-markovian phonon-induced decoherence, Phys. Rev. B **87**, 081308 (2013).

[17] C. Gustin and S. Hughes, Influence of electron-phonon scattering for an on-demand quantum dot single-photon source using cavity-assisted adiabatic passage, Phys. Rev. B **96**, 085305 (2017).

[18] T. Grange, N. Somaschi, C. Antón, L. De Santis, G. Coppola, V. Giesz, A. Lemaître, I. Sagnes, A. Auffèves, and P. Senellart, Reducing Phonon-Induced Decoherence in Solid-State Single-Photon Sources with Cavity Quantum Electrodynamics, Phys. Rev. Lett. **118**, 253602 (2017).

[19] D. P. S. McCutcheon, N. S. Dattani, E. M. Gauger, B. W. Lovett, and A. Nazir, A general approach to quantum dynamics using a variational master equation: Application to phonon-damped Rabi rotations in quantum dots, Phys. Rev. B **84**, 081305 (2011).

[20] R. Manson, K. Roy-Choudhury, and S. Hughes, Polaron master equation theory of pulse-driven phonon-assisted population inversion and single-photon emission from quantum-dot excitons, Phys. Rev. B **93**, 155423 (2016).

[21] A. Nazir and D. P. S. McCutcheon, Modelling exciton–phonon interactions in optically driven quantum dots, J. Phys. Condens. Matter **28**, 103002 (2016).

[22] D. E. Reiter, Time-resolved pump-probe signals of a continuously driven quantum dot affected by phonons, Phys. Rev. B **95**, 125308 (2017).

[23] P. Machnikowski, Theory of two-photon processes in quantum dots: Coherent evolution and phonon-induced dephasing, Phys. Rev. B **78**, 195320 (2008).

[24] K. Gawarecki, S. Lüker, D. E. Reiter, T. Kuhn, M. Glässl, V. M. Axt, A. Grodecka-Grad, and P. Machnikowski, Dephasing in the adiabatic rapid passage in quantum dots: Role of phonon-assisted biexciton generation, Phys. Rev. B **86**, 235301 (2012).

[25] J. Förstner, C. Weber, J. Danckwerts, and A. Knorr, Phonon-Assisted Damping of Rabi Oscillations in Semiconductor Quantum Dots, Phys. Rev. Lett. **91**, 127401 (2003).

[26] A. Krügel, V. M. Axt, T. Kuhn, P. Machnikowski, and A. Vagov, The role of acoustic phonons for Rabi oscillations in semiconductor quantum dots, Appl. Phys. B **81**, 897 (2005).

[27] S. Lüker, K. Gawarecki, D. E. Reiter, A. Grodecka-Grad, V. M. Axt, P. Machnikowski, and T. Kuhn, Influence of acoustic phonons on the optical control of quantum dots driven by adiabatic rapid passage, Phys. Rev. B **85**, 121302 (2012).

[28] D. E. Reiter, S. Lüker, K. Gawarecki, A. Grodecka-Grad, P. Machnikowski, V. M. Axt, and T. Kuhn, Phonon effects on population inversion in quantum dots: Resonant, detuned and frequency-swept excitations, Acta Phys. Pol. A **122**, 1065 (2012).

[29] A. Vagov, M. D. Croitoru, M. Glässl, V. M. Axt, and T. Kuhn, Real-time path integrals for quantum dots: Quantum dissipative dynamics with superohmic environment coupling, Phys. Rev. B **83**, 094303 (2011).

[30] M. Glässl, A. Vagov, S. Lüker, D. E. Reiter, M. D. Croitoru, P. Machnikowski, V. M. Axt, and T. Kuhn, Long-time dynamics and stationary nonequilibrium of an optically driven strongly confined quantum dot coupled to phonons, Phys. Rev. B **84**, 195311 (2011).

[31] M. Glässl, M. D. Croitoru, A. Vagov, V. M. Axt, and T. Kuhn, Influence of the pulse shape and the dot size on the decay and reappearance of Rabi rotations in laser driven quantum dots, Phys. Rev. B **84**, 125304 (2011).

[32] U. Woggon, *Optical Properties of Semiconductor Quantum Dots* (Springer, Berlin, 1997).

[33] P. W. Fry, I. E. Itskevich, S. R. Parnell, J. J. Finley, L. R. Wilson, K. L. Schumacher, D. J. Mowbray, M. S. Skolnick, M. Al-Khafaji, A. G. Cullis, M. Hopkinson, J. C. Clark, and G. Hill, Photocurrent spectroscopy of InAs/GaAs self-assembled quantum dots, Phys. Rev. B **62**, 16784 (2000).

[34] D. Wigger, D. E. Reiter, V. M. Axt, and T. Kuhn, Fluctuation properties of acoustic phonons generated by ultrafast optical excitation of a quantum dot, Phys. Rev. B **87**, 085301 (2013).

[35] D. Wigger, S. Lüker, D. E. Reiter, V. M. Axt, P. Machnikowski, and T. Kuhn, Energy transport and coherence properties of acoustic phonons generated by optical excitation of a quantum dot, J. Phys. Condens. Matter **26**, 255802 (2014).

[36] G. M. Vanacore, J. Hu, W. Liang, S. Bietti, S. Sanguinetti, F. Carbone, and A. H. Zewail, Ultrafast atomic-scale visualization of acoustic phonons generated by optically excited quantum dots, Struct. Dyn. **4**, 044034 (2017).

[37] B. Krummheuer, V. M. Axt, T. Kuhn, I. D'Amico, and F. Rossi, Pure dephasing and phonon dynamics in GaAs- and GaN-based quantum dot structures: Interplay between material parameters and geometry, Phys. Rev. B **71**, 235329 (2005).

[38] A. Krügel, V. M. Axt, and T. Kuhn, Back action of nonequilibrium phonons on the optically induced dynamics in semiconductor quantum dots, Phys. Rev. B **73**, 035302 (2006).

[39] T. Calarco, A. Datta, P. Fedichev, E. Pazy, and P. Zoller, Spin-based all-optical quantum computation with quantum dots: Understanding and suppressing decoherence, Phys. Rev. A **68**, 012310 (2003).

[40] D. P. S. McCutcheon and A. Nazir, Quantum dot Rabi rotations beyond the weak exciton–phonon coupling regime, New J. Phys **12**, 113042 (2010).

[41] B. Krummheuer, V. M. Axt, and T. Kuhn, Theory of pure dephasing and the resulting absorption line shape in semiconductor quantum dots, Phys. Rev. B **65**, 195313 (2002).

[42] K. Huang and A. Rhys, Theory of light absorption and nonradiative transitions in *F*-centres, Proc. R. Soc. London (A) **204**, 406 (1950).

[43] C. B. Duke and G. D. Mahan, Phonon-Broadened Impurity Spectra. I. Density of States, Phys. Rev. **139**, A1965 (1965).

[44] A. J. Ramsay, T. M. Godden, S. J. Boyle, E. M. Gauger, A. Nazir, B. W. Lovett, A. M. Fox, and M. S. Skolnick, Phonon-Induced Rabi-Frequency Renormalization of Optically Driven Single InGaAs/GaAs Quantum Dots, Phys. Rev. Lett. **105**, 177402 (2010).

[45] A. Vagov, M. D. Croitoru, V. M. Axt, T. Kuhn, and F. M. Peeters, Nonmonotonic Field Dependence of Damping and Reappearance of Rabi Oscillations in Quantum Dots, Phys. Rev. Lett. **98**, 227403 (2007).

[46] D. P. S. McCutcheon and A. Nazir, Coherent and incoherent dynamics in excitonic energy transfer: Correlated fluctuations and off-resonance effects, Phys. Rev. B **83**, 165101 (2011).

[47] Y. Wu, I. M. Piper, M. Ediger, P. Brereton, E. R. Schmidgall, P. R. Eastham, M. Hugues, M. Hopkinson, and R. T. Phillips, Population Inversion in a Single InGaAs Quantum Dot using the Method of Adiabatic Rapid Passage, Phys. Rev. Lett. **106**, 067401 (2011).

[48] C. M. Simon, T. Belhadj, B. Chatel, T. Amand, P. Renucci, A. Lemaitre, O. Krebs, P. A. Dalgarno, R. J. Warburton, X. Marie, and B. Urbaszek, Robust Quantum Dot Exciton Generation via Adiabatic Passage with Frequency-Swept Optical Pulses, Phys. Rev. Lett. **106**, 166801 (2011).

[49] F. J. R. Schülein, E. Zallo, P. Atkinson, O. G. Schmidt, R. Trotta, A. Rastelli, A. Wixforth, and H. J Krenner, Fourier synthesis of radiofrequency nanomechanical pulses with different shapes, Nat. Nanotechnol. **10**, 512 (2015).

[50] B. Villa, A. J. Bennett, D. J. P. Ellis, J. P. Lee, J. Skiba-Szymanska, T. A. Mitchell, J. P. Griffiths, I. Farrer, D. A. Ritchie, C. J. B. Ford, and A. J. Shields, Surface acoustic wave modulation of a coherently driven quantum dot in a pillar microcavity, Appl. Phys. Lett. **111**, 011103 (2017).

[51] T. Czerniuk, D. Wigger, A. V. Akimov, C. Schneider, M. Kamp, S. Höfling, D. R. Yakovlev, T. Kuhn, D. E. Reiter, and M. Bayer, Picosecond Control of Quantum Dot Laser Emission by Coherent Phonons, Phys. Rev. Lett. **118**, 133901 (2017).